Direct Probe of Vibrational Fingerprint and Combination Band Coupling

Ryan P. McDonnell, Kelson Oram, Mark A. Boyer, Daniel D. Kohler, Kent A. Meyer, Edwin L. Sibert III, and John C. Wright*

Department of Chemistry and Theoretical Chemistry Institute, University of Wisconsin - Madison, Madison, WI 53706, United States of America

E-mail: wright@chem.wisc.edu

March 7, 2024

Abstract

Vibrational fingerprints and combination bands are a direct measure of couplings that control molecular properties. However, most combination bands possess small transition dipoles. Here, we use multiple, ultrafast coherent infrared pulses to resolve vibrational coupling between CH_3CN fingerprint modes at 918, 1039 cm^{-1} and combination bands in the 2750-6100 cm^{-1} region via doubly vibrationally enhanced (DOVE) coherent multidimensional spectroscopy (CMDS). This approach provides a direct probe of vibrational coupling between fingerprint modes and near infrared combination bands of large and small transition dipoles in a molecular system over a 3350 cm^{-1} range.

TOC Graphic

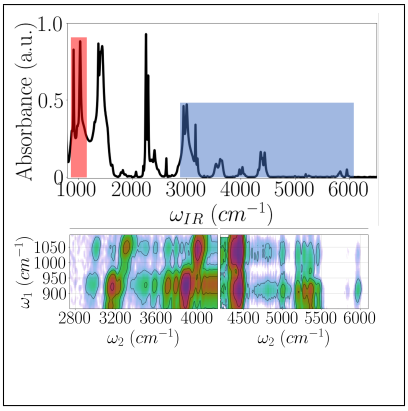

Coherent multidimensional spectroscopy (CMDS) has the capability to resolve the identity of vibrational overtones and combination bands.[1–3] Combination bands and overtones are commonly assigned by comparing their near infrared (NIR) frequencies to sums of harmonic frequencies evaluated using *ab initio* electronic structure methods, such as density functional theory (DFT).[4–6] An alternative method to assign combination bands is through correlations found in multidimensional spectra.[7] These correlation can ease the dependence of spectral assignments on DFT approaches. However, it is often difficult to probe overtones and combination bands through ultrafast spectroscopy due to their smaller transition dipole moments.[8–11] Overtone and combination band transitions are forbidden and are observed because of coupling between modes. This coupling makes overtones and combination bands very important because they are a direct measure of the anharmonicity of modes that can drive chemical reactions. This letter demonstrates how CMDS can directly probe vibrational couplings between fundamental, fingerprint modes with overtones and combination bands whose vibrational transition dipole moments vary over roughly two orders of magnitude. We use doubly vibrationally enhanced (DOVE) CMDS to create a superposition of vibrational states and probe these vibrational couplings.[12] In DOVE-CMDS, two tunable infrared pulses are used: one to excite a high-energy vibration (ω_2) and another to excite or de-excite a low-energy fundamental (or fingerprint) mode (ω_1). A third, final optical pulse (ω_3) stimulates a Raman output transition (ω_4).[12–14] The superposition emits multiple output beams with directions and frequencies controlled by momentum ($\hbar\vec{k}$) and energy ($\hbar\omega$) conservation. We create spectra by measuring the intensity of the $\vec{k}_4 = -\vec{k}_1 + \vec{k}_2 + \vec{k}_3$ output beam as the infrared frequencies are scanned across vibrational resonances. In the electric dipole approximation, spectral peaks result when the two vibrational states are coupled in expansions of the potential energy surface and/or molecular electric dipole moment.[15] Interference from non-resonant background often determines the detection limits.[16,17] With ultrafast laser systems where pulse durations rival the vibrational coherence times, such contributions can be effectively removed, at the cost of spectral resolution, by separating the pulses in time.[18,19]

Through typical perturbative methods,[20,21] DOVE signal can be diagrammed through the following Liouville pathways:[12,22,23]

$$|g\rangle\langle g| \overset{1}{\Rightarrow} |g\rangle\langle v| \overset{2}{\Rightarrow} |v''\rangle\langle v| \overset{3}{\Rightarrow} |e\rangle\langle v| \overset{4}{\Rightarrow} |v\rangle\langle v| \tag{1a}$$

$$|g\rangle\langle g| \overset{2}{\Rightarrow} |v''\rangle\langle g| \overset{1}{\Rightarrow} |v''\rangle\langle v| \overset{3}{\Rightarrow} |e\rangle\langle v| \overset{4}{\Rightarrow} |v\rangle\langle v| \tag{1b}$$

$$|g\rangle\langle g| \overset{2}{\Rightarrow} |v''\rangle\langle g| \overset{1}{\Rightarrow} |v'\rangle\langle g| \overset{3}{\Rightarrow} |e\rangle\langle g| \overset{4}{\Rightarrow} |g\rangle\langle g| \tag{1c}$$

where the numbers define the interacting pulse, $|g\rangle, |e\rangle$ are ground and virtual states, and $|v\rangle, |v'\rangle, |v''\rangle$ are vibrational states. In this work, we choose $|v\rangle$ to be a low energy fundamental mode and $|v'\rangle, |v''\rangle$ are high energy vibrations that can correspond to a fundamental, overtone or combination band. These pathways are diagrammed in Figure 1. The pathways involve a multi-quantum vibrational transition; either a ω_2 transition to a combination band ($v'' = v' + v$) or, in cases where v'' is not composed of v' or v, a multi-quantum Raman transition with ω_3. Due to anharmonicity, multi-quantum transitions are generally weak. The signal from these pathways is described by the third-order electrical susceptibility tensor, $\chi^{(3)}_{IJKL}$, where the subscript indices denote Cartesian coordinates in the laboratory frame. In the 1-2-3 time ordering, the peak susceptibility scales as

$$\chi^{(3)}_{IJKL} \sim \langle \alpha_3 \mu_2 \mu_1 \rangle_{IJKL} \tag{2a}$$

and in the 1-2-3 time ordering, the peak susceptibility scales as

$$\chi^{(3)}_{IJKL} \sim \langle \alpha_3 \mu_1 \mu_2 \rangle_{IJKL} \tag{2b}$$

where α_3 is a Raman polarizability induced by ω_3, and μ_n is the transition dipole probed by ω_n. The brackets denote a rotational average of the transition elements due to the sample's isotropic nature.[26,27] All excitations are vertically polarized, so we isolate $\chi^{(3)}_{ZZZZ}$.

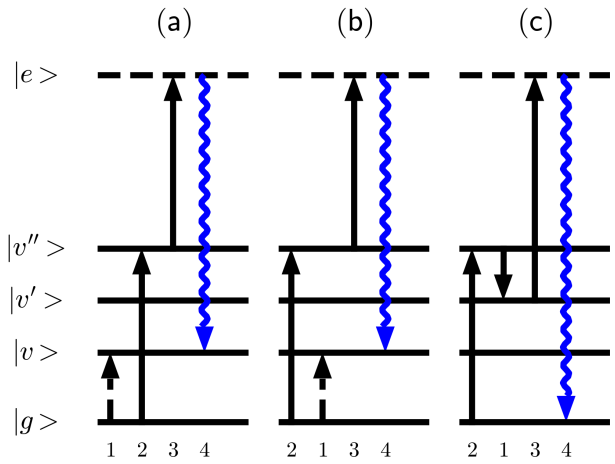

Figure 1: Wave Mixing Energy Level (WMEL) diagrams[24] of (a,b) DOVE-IR, (c) DOVE-Raman coherence pathways used in this work. These correspond to the pathways described by Equation 1.[25] $|v\rangle, |v'\rangle, |v''\rangle$ denote vibrational states on the ground electronic manifold; $|e\rangle$ denotes a virtual state. Solid and dotted arrows indicate ket and bra side transitions, respectively. Interaction times are ordered from left to right. Pulse labeling denotes frequency, not interaction time. The output frequency, ω_4 (blue line), is defined as $\omega_4 = -\omega_1 + \omega_2 + \omega_3$. Time delays, τ_{ij}, are defined as $\tau_{ij} = \tau_i - \tau_j$. In this work, the infrared pulse time delays are referenced to the optical upconversion pulse (ω_3).

The homodyne-detected output scales as the square of the susceptibility, $|\chi^{(3)}_{ZZZZ}|^2$.

In this letter, we probe coupling between the fingerprint and combination modes of acetonitrile (CH_3CN). CH_3CN is a prototypical molecule commonly used to expand the methods of nonlinear spectroscopy.[12,28–31] Fourier transform infrared (FT-IR) spectroscopy of CH_3CN shows strongly absorbing ν(CC) stretch (918 cm^{-1}) and $\rho(CH_3)$ rocking (1039 cm^{-1}) fingerprint modes (Figure 2), while the absorption of most combination modes are roughly one to two orders of magnitude smaller.[32] The DOVE-CMDS spectra resolve a multitude of combination bands coupled to these fundamentals. Fingerprint-selective coupling can help assess the composition of combination bands. The spectra show peaks across a dynamic range of four orders of magnitude, showing DOVE-CMDS is sensitive to weak coupling between modes that do not share a coupled vibration. We attribute this sensitivity to several factors, including: (1) the use of pulse delays to minimize non-resonant background, (2) the use of a neat solvent as an analyte, (3) sample path length and (4) single photon

output sensitivity. Non-resonant background and absorption effects can obfuscate even the strongest spectral features.[33] Resonant signal undergoes free induction decay (FID), and therefore persists longer than non-resonant signal. While pulse delays reduce signal due to FID, it will also suppress non-resonant background relative to the resonant signal.[18,34] A relatively short sample pathlength (60 μm) was used to avoid absorption induced phase mismatch effects.[33,35–37]

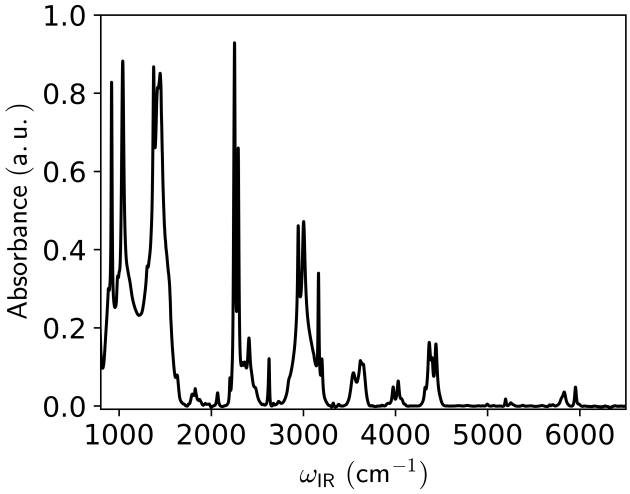

Figure 2: Baseline corrected FT-IR spectrum of neat CH_3CN used in this work.

The DOVE-CMDS spectra show the coupling of the ν(CC) $\rho(CH_3)$ fingerprint modes with high energy vibrations in the 2750-6100 cm^{-1} range (Figure 3). The peak frequencies correspond well to those in the infrared absorption spectrum (Figure 2), and we are able to match features to previously assigned vibrations (Table S1).[38]

Figures 3a and 3c reveal the mode couplings within the 2750 cm^{-1} $\leq \omega_2 \leq$ 4200 cm^{-1} range using the 1-2-3 pulse sequence (cf. Figure 1a). To understand the relationship between CH_3CN vibrational couplings and the 2D features, we first examine the symmetric and asymmetric CH stretch modes, $\nu(CH)_s$ (2944 cm^{-1}) and $\nu(CH)_{as}$ (3003 cm^{-1}), respectively (Table 1). These ν(CH) modes are thought to be significant contributors to CH_3CN combination modes.[38] If coupling between the fingerprint modes and $\nu(CH)_s$, $\nu(CH)_{as}$ is present, then cross peaks at (ω_1, 2945) cm^{-1} and (ω_1, 3000) cm^{-1} should be present in the 2D DOVE

spectrum. Indeed, features at $(\omega_1, \omega_2) = (920, 2945)$ cm^{-1} and $(1040, 3000)$ cm^{-1} are present (Figure 3). Note that ν(CC), $\nu(\mathrm{CH})_\mathrm{s}$ and $\rho(\mathrm{CH_3})$, $\nu(\mathrm{CH})_\mathrm{as}$ share common symmetry (A_1, E, respectively), which likely explains why $\nu(\mathrm{CH})_\mathrm{s}$ does not couple to $\rho(\mathrm{CH_3})$.[15,38] Note that all symmetry arguments are based upon an isolated CH_3CN molecule, which belongs to the C_{3v} point group.

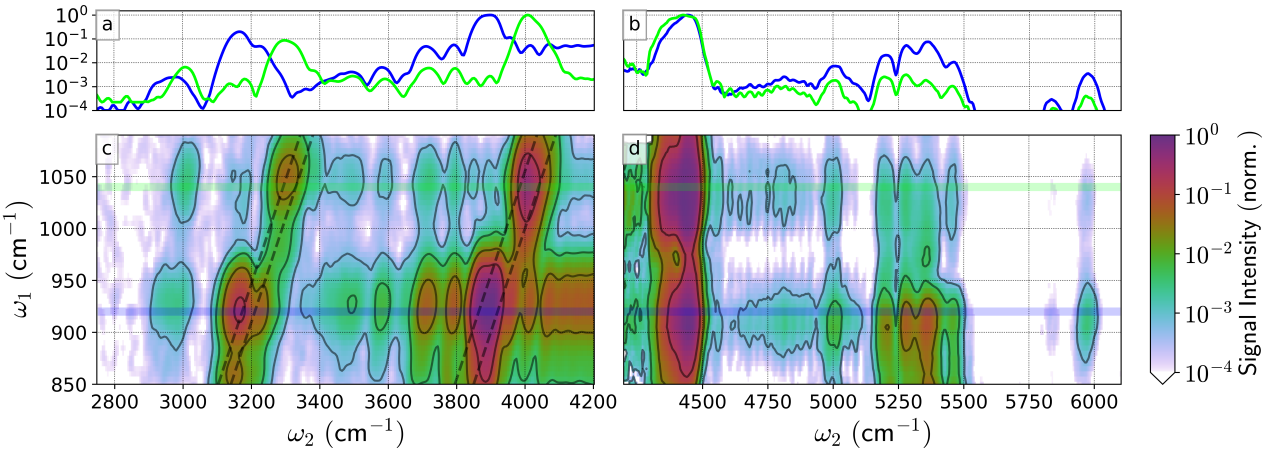

Figure 3: DOVE-CMDS Spectra of neat CH_3CN. 1D slices taken along ω_1 = 920 cm^{-1} (blue), 1040 cm^{-1} (green) where (a) τ_{13} = -1.5 ps, τ_{23}= -0.5 ps; (b) τ_{13} = -0.5 ps, τ_{23}= -1.0 ps. Full 2D Spectra at (c) $\omega_2 \otimes \omega_1$ = [2750, 4200] cm^{-1} $\otimes$ [850, 1090] cm^{-1}, τ_{13} = -1.5 ps, τ_{23}= -0.5 ps; (d) $\omega_2 \otimes \omega_1$ = [4200, 6100] cm^{-1} $\otimes$ [850, 1090] cm^{-1}; τ_{13} = -0.5 ps, τ_{23}= -1.0 ps. ω_3= 22222 cm^{-1} (450 nm) for all spectra. The spectra are smoothed and corrected for frequency-dependent power fluctuations. White pixels indicate intensities less than 10^{-4}. Dotted lines indicate combination bands that share a common mode.

Table 1: Relevant CH_3CN normal modes with central frequencies obtained from an FT-IR Spectrum (Figure 2). Assignments and symmetries are taken from Pace and Noe.[39]

Normal Mode	Frequency (cm^{-1})	Symmetry
ν(CC)	918	A_1
$\rho(\mathrm{CH_3})$	1039	E
$\delta(\mathrm{CH_3})_\mathrm{s}$	1374	A_1
$\delta(\mathrm{CH_3})_\mathrm{as}$	1443	E
ν(CN)	2253	A_1
$\nu(\mathrm{CH})_\mathrm{s}$	2944	A_1
$\nu(\mathrm{CH})_\mathrm{as}$	3003	E

When ω_1 excites a fingerprint mode, $|v\rangle$, a coupled combination mode, $|v''\rangle = |v\rangle + |s\rangle$, may be selectively amplified in the ω_2 spectrum. When multiple fingerprints couple to the

same mode, $|s\rangle$, and assuming minimal wavefunction mixing (i.e., no Fermi resonance nor Darling-Dennison resonance),[40,41] the amplified combination mode will shift with the fundamental as $\omega_2 = \omega_1 + \omega_s$, and the 2D resonances will lie along a diagonal line. Since the DOVE pathways eliminate the $|s\rangle$ quantum through the Raman transition with ω_3 (see Figures 1a,b), a shared mode must be Raman active to be bright. In Figure 3c we identify peaks lying along four diagonal trend lines denoted by dotted lines. From left to right, the diagonal lines imply shared modes of approximate energy $\omega_s \sim 2250, 2290, 2940,$ and 3000 cm^{-1}, which can each be assigned to the Raman-active modes $\nu(\text{CN}), \delta(\text{CH}_3)_s + \nu(\text{CC}), \nu(\text{CH})_s,$ and $\nu(\text{CH})_{as}$, respectively.

The (ν(CC), ν(CN) + ν(CC)) cross peak is useful because the peak susceptibility can be calculated from known IR absorption and spontaneous Raman scattering data.[42,43] We calculate a peak susceptibility of $\sim 1\times 10^{-13}$ cm^3 erg^{-1} for this feature. See the Supporting Materials for calculation details, including a treatment of orientational averaging. The calculated susceptibility quantifies signal sensitivity. The peak susceptibility is similar to the maximum susceptibility seen in nanosecond DOVE-CMDS measurements, but the dynamic range of susceptibilities in those experiments were limited, by nonresonant background, to $\sim$10:1.[12,13] Our calculated susceptibility assumes pulse overlap and does not account for the loss of signal through our delayed pulse sequence.[18,19] The attenuation value depends on the dephasing rates;[18] we estimate this attenuation factor to be ~ 10.

Alternatively, if many fingerprint modes couple to a high energy mode $|v''\rangle$, the amplified combination mode is a fixed frequency, and 2D resonances will lie along vertical lines at $\omega_2 = \omega_{v''}$, where $\omega_{v''}$ is the frequency of $|v''\rangle$. These features are not fingerprint selective. The stronger, structured vertical features are indicative of modes that are coupled to both ν(CC) and $\rho(\text{CH}_3)$, along with other fundamentals. For example, consider the features at (920 cm^{-1}, 3790 cm^{-1}) and (1040 cm^{-1}, 3790 cm^{-1}). The mode at 3790 cm^{-1} is likely due to a $2\delta(\text{CH}_3)_{\text{as}} + \nu(\text{CC})$ combination band, resulting in the relatively strong coupling along $\omega_1 = 920$ cm^{-1}. In addition, the $2\delta(\text{CH}_3)_{\text{as}}$ mode possesses both A_1 and E symmetry.[38]

The mixed symmetry of $2\delta(CH_3)_{as}$ provides an avenue for coupling between $\rho(CH_3)$ and $2\delta(CH_3)_{as} + \nu(CC)$,[15] likely resulting in the structured vertical feature at $\omega_2 = 3790$ cm^{-1}.

Interference from singly-resonant processes can obfuscate the doubly-resonant cross peaks.[16,43] For $\omega_2 > 4200$ cm^{-1}, we found it difficult to isolate CH_3CN DOVE-CMDS output from these singly resonant processes (Figure S6) using the 1-2-3 pulse sequence, as discussed in the supporting information. To avoid these effects, spectra for $\omega_2 > 4200$ cm^{-1} were acquired in the 2-1-3 pulse sequence (Figure 1b,c). In the 2-1-3 pulse sequence, there is interference between DOVE-IR (Figure 1b) and DOVE-Raman (Figure 1c), a vibrational analogue of doubly resonant coherent anti-Stokes Raman spectroscopy.[25,44] We suspect this interference is responsible for the lack of diagonal cross peak patterns in the 2-1-3 pulse sequence.[45] This interference, along with the relative proportion of transition dipole strengths, strongly suppresses the singly resonant contribution. Additionally, as discussed in the supplementary information, singly resonant features are not expected to significantly contribute to overall output in the 2-1-3 pulse ordering.

It is important to note that transition dipole moments of modes in the 5000 cm^{-1} region are roughly two orders of magnitude smaller than $\nu(CC)$.[32] Weak modes in a FT-IR spectrum can be enhanced in a DOVE-CMDS spectrum by coupling to a mode with a stronger transition dipole moment (Figures 3b, 3d). Similar results have been observed in triply resonant experiments.[46] Thus, Figure 3 demonstrates that DOVE-CMDS can probe coupling between the $\nu(CC)$ and $\rho(CH_3)$ fingerprint modes and combination bands of varying transition dipole moments throughout the near infrared.

Figure 3a suggests $\nu(CC)$ and $\rho(CH_3)$ couples with the CH stretch fundamentals, $\nu(CH)_s$, $\nu(CH)_{as}$. However, previous population dynamics studies showed any feeding to $\nu(CC)$ from the $\nu(CH)_s$, $\nu(CH)_{as}$ modes in CH_3CN required an intermediate step whose lifetime is on the scale of tens of ps.[29] As such, it appears DOVE-CMDS can probe small, off-diagonal terms in anharmonic potential energy surfaces, akin to other CMDS methods.[47,48] Future studies that investigate IR-pump-DOVE-CMDS-probe, analogous to IR-pump-sum frequency-probe,

experiments on these modes in CH_3CN could resolve this coupling in more detail.[49,50]

To further investigate how ν(CC) and $\rho(CH_3)$ couple to $\nu(CH)_s$, $\nu(CH)_{as}$, we examines the coupling of ν(CC) and $\rho(CH_3)$ to the CH stretch overtones. Figure 4 shows the region of Figure 3d with ω_2 excitation near twice the energy of $\nu(CH)_s$, $\nu(CH)_{as}$. The NIR absorption spectrum (Figure 2) shows two prominent modes that match those seen in the 2D DOVE-CMDS spectrum (Figure 4). Previous analysis has suggested the primary composition of these modes are the 2ν(CH) overtones,[38,51] though it is possible there are other contributions.

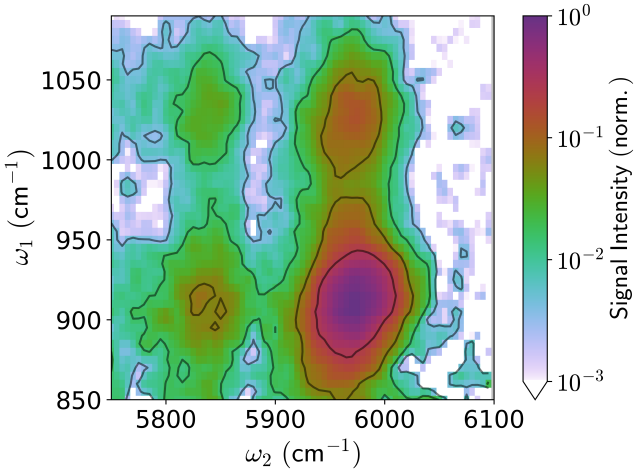

Figure 4: Same as Figure 3d, but zoomed in on the $\omega_2 \otimes \omega_1$ = [5750, 6100] cm^{-1} $\otimes$ [850, 1090] cm^{-1} region. τ_{13} = -0.5 ps, τ_{23}= -1.0 ps. The spectrum is normalized to the intensity of the (920, 5970) cm^{-1} feature.

Since the ν(CC), $\rho(CH_3)$ modes are roughly 5000 cm^{-1} apart in energy relative to 2ν(CH), and do not share common oscillators, it is surprising that coupling between these modes can be resolved. To glean insight into this coupling, second-order vibrational perturbation theory (VPT2) calculations were performed using a quartic force-field evaluated at the B3LYP/aug-cc-pVDZ level of theory/basis using the `Gaussian 16` software package and the `PyVibPTn` implementation of VPT2.[52–59] The B3LYP density functional has provided satisfactory results in previous computational studies of CH_3CN.[15,60] Calculations were performed on an isolated, gas phase CH_3CN molecule, sufficient to describe DOVE-CMDS spectra of CH_3CN.[15,45]

At the B3LYP/aug-cc-pVDZ level of theory/basis, the calculations give a coupling be-

tween ν(CC) and the 2ν(CH) modes of less than 1 cm^{-1}. A similar calculation shows the coupling between ν(CC) and ν(CC) + ν(CN) is roughly 60 cm^{-1}. See the supporting information for more details of the calculations. The output from the (920, 5970) cm^{-1} feature is nearly three orders of magnitude less intense than the strongest feature present in Figure 3. The subwavenumber coupling between ν(CC) and the 2ν(CH) modes extracted from VPT2 calculations suggest that higher order terms in the potential energy surface and dipole moments likely contribute to the observed signal. Since DOVE-CMDS appears to resolve this higher order coupling, DOVE-CMDS could possibly be used as a probe of resolving weak, off-diagonal vibrational mode couplings.

Though this work studied a model molecular system, the use of DOVE-CMDS to identify and isolate coupling between fingerprint modes and weak combination modes may be extended to aid in large molecular structure determination. Combination band anharmonicities can inform on intermolecular interactions and aid in protein structure determination.[61] Polarization schemes can be imposed to extract coupling between specific molecular conformers and vibrational modes.[27,62] Guo et al. have demonstrated the feasibility of probing intermolecular coupling through DOVE-CMDS.[62] Use of an electronically resonant third pulse would provide deeper insight into the electronic structure of intermolecular interactions, vibrational coupling between modes with exceptionally small transition dipole moments, and increase signal by orders of magnitude.[46,63–65] The application of DOVE-CMDS and other vibrational/electronic spectroscopies to large molecules could assist in spectral and structure determination.

In summary, we probed coupling between fingerprint and combination/overtone mode vibrations in CH_3CN via DOVE-CMDS over a range of 3000 cm^{-1}. We demonstrated that a fingerprint mode with a large transition dipole can be coupled to numerous modes throughout the mid and near infrared with transition dipole moments that vary over at least two orders of magnitude. Methods to assign combination bands through vibrational correlations through diagonal peaks in the DOVE-CMDS spectra were identified. This methodology can be

applied towards understanding the complex infrared spectra of biomolecular and materials systems, whose infrared spectra possess many combination modes and overtones, but also understanding non-covalent interactions and energy transfer mechanisms, as examples.[29,62] Overall, we have demonstrated that ultrafast laser technology has advanced to a point where multidimensional, frequency domain spectroscopies can provide unprecedented insight into understanding vibrational coupling throughout most of the infrared region.

Acknowledgement

We thank Prof. Peter C. Chen for useful discussions and Prof. Wei Zhao for sharing hyperpolarizability data. This work received support from the National Science Foundation (NSF) (Grant Nos. CHE-1900095 and CHE-2203290). R.P.M. gratefully acknowledges support from the NSF Graduate Research Fellowship Program (Grant no. DGE-2137424).

Supporting Information Available

See Supplemental Material at [URL will be inserted by publisher] for Methods, Materials Characterization, Description of and Results from Vibrational Perturbation Theory, Orientational Averaging, Additional Discussion on Singly Vibrationally Enhanced Processes. The data and workup scripts that support this study are permissively licensed and available for reuse at https://osf.io/xjeuy/.

References

(1) Carlson, R. J.; Nguyen, D. C.; Wright, J. C. Analysis of vibronic mode coupling in pentacene by fully resonant coherent four-wave mixing. *Journal of Chemical Physics* **1990**, *92*, 1538–1546, DOI: 10.1063/1.458084.

(2) Boyle, E. S.; Pakoulev, A. V.; Wright, J. C. Fully Coherent Triple Sum Frequency

Spectroscopy of a Benzene Fermi Resonance. *Journal of Physical Chemistry A* **2013**, *117*, 5578–5588, DOI: 10.1021/jp404713x.

(3) Daniels, D. A.; Wells, T. A.; Chen, P. C. High resolution two-dimensional infrared (HR-2DIR) spectroscopy of gas phase molecules. *Journal of Chemical Physics* **2022**, *157*, 184201, DOI: 10.1063/5.0109084.

(4) Franke, P. R.; Stanton, J. F.; Douberly, G. E. How to VPT2: Accurate and Intuitive Simulations of CH Stretching Infrared Spectra Using VPT2+K with Large Effective Hamiltonian Resonance Treatments. *Journal of Physical Chemistry A* **2021**, *125*, 1301–1324, DOI: 10.1021/acs.jpca.0c09526.

(5) Barone, V.; Alessandrini, S.; Biczysko, M.; Cheeseman, J. R.; Clary, D. C.; McCoy, A. B.; DiRisio, R. J.; Neese, F.; Melosso, M.; Puzzarini, C. Computational molecular spectroscopy. *Nature Reviews Methods Primers* **2021**, *1*, 38, DOI: 10.1038/s43586-021-00034-1.

(6) Sibert, E. L. Modeling Anharmonic Effects in the Vibrational Spectra of High-Frequency Modes. *Annual Review of Physical Chemistry* **2023**, *74*, 219–244, DOI: 10.1146/annurev-physchem-062422-021306.

(7) Carlson, R. J.; Wright, J. C. Analysis of vibrational correlations and couplings in the lowest two singlet states of pentacene by high resolution, fully resonant, coherent four-wave mixing spectroscopy. *Journal of Chemical Physics* **1990**, *92*, 5186–5195, DOI: 10.1063/1.458553.

(8) Kurochkin, D. V.; Naraharisetty, S. R. G.; Rubtsov, I. V. Dual-frequency 2D IR on interaction of weak and strong IR modes. *Journal of Physical Chemistry A* **2005**, *109*, 10799–10802, DOI: 10.1021/jp055811+.

(9) Isaienko, O.; Nihonyanagi, S.; Sil, D.; Borguet, E. Observation of the Bending Mode of Interfacial Water at Silica Surfaces by Near-Infrared Vibrational Sum-Frequency

Generation Spectroscopy of the Stretch plus Bend Combination Bands. *Journal of Physical Chemistry Letters* **2013**, *4*, 531–535, DOI: 10.1021/jz3015088.

(10) Wright, J. C. Fundamental Studies of Relationships between Experimental Nonlinear Coherent Vibrational Spectroscopies. *Journal of Physical Chemistry Letters* **2019**, *10*, 2767–2774, DOI: 10.1021/acs.jpclett.9b01280.

(11) Altman, R. M.; Richmond, G. L. Twist and Stretch: Assignment and Surface Charge Sensitivity of a Water Combination Band and Its Implications for Vibrational Sum Frequency Spectra Interpretations. *The Journal of Physical Chemistry B* **2021**, *125*, 6717–6726, DOI: 10.1021/acs.jpcb.1c03408.

(12) Zhao, W.; Wright, J. C. Measurement of $\chi^{(3)}$ for Doubly Vibrationally Enhanced Four Wave Mixing Spectroscopy. *Physical Review Letters* **1999**, *83*, 1950–1953, DOI: 10.1103/PhysRevLett.83.1950.

(13) Zhao, W.; Wright, J. C. Doubly vibrationally enhanced four wave mixing: The optical analog to 2D NMR. *Physical Review Letters* **2000**, *84*, 1411–1414, DOI: 10.1103/PhysRevLett.84.1411.

(14) Kirkwood, J. C.; Ulness, D. J.; Albrecht, A. C. On the classification of the electric field spectroscopies: Application to Raman scattering. *Journal of Physical Chemistry A* **2000**, *104*, 4167–4173, DOI: 10.1021/jp992542c.

(15) Kwak, K.; Cha, S.; Cho, M.; Wright, J. C. Vibrational interactions of acetonitrile: Doubly vibrationally resonant IR-IR-visible four-wave-mixing spectroscopy. *Journal of Chemical Physics* **2002**, *117*, 5675–5687, DOI: 10.1063/1.1501129.

(16) LaBuda, M. J.; Wright, J. C. Measurement of vibrationally resonant $\chi^{(3)}$ and the feasibility of new vibrational spectroscopies. *Physical Review Letters* **1997**, *79*, 2446–2449, DOI: 10.1103/PhysRevLett.79.2446.

(17) Meyer, K. A.; Wright, J. C. Detection limits for time-resolved coherent two-dimensional vibrational spectroscopy. *Analytical Chemistry* **2001**, *73*, 5020–5025, DOI: 10.1021/ac0107195.

(18) Meyer, K. A.; Wright, J. C. Interference, dephasing, and coherent control in time-resolved frequency domain two-dimensional vibrational spectra. *Journal of Physical Chemistry A* **2003**, *107*, 8388–8395, DOI: 10.1021/jp035146+.

(19) Kohler, D. D.; Thompson, B. J.; Wright, J. C. Frequency-domain coherent multidimensional spectroscopy when dephasing rivals pulsewidth: Disentangling material and instrument response. *Journal of Chemical Physics* **2017**, *147*, 084202, DOI: 10.1063/1.4986069.

(20) Yee, T. K.; Gustafson, T. K. Diagrammatic analysis of the density operator for nonlinear optical calculations: Pulsed and cw responses. *Phys. Rev. A* **1978**, *18*, 1597–1617, DOI: 10.1103/PhysRevA.18.1597.

(21) Oudar, J. L.; Shen, Y. R. Nonlinear spectroscopy by multiresonant four-wave mixing. *Physical Review A* **1980**, *22*, 1141–1158, DOI: 10.1103/PhysRevA.22.1141.

(22) Mukamel, S. Nonimpact unified theory of four-wave mixing and two-photon processes. *Physical Review A* **1983**, *28*, 3480–3492, DOI: 10.1103/PhysRevA.28.3480.

(23) Carlson, R. J.; Wright, J. C. Diagrammatic calculation of resonant optical susceptibilities in the presence of excited-state populations and population feeding. *Physical Review A* **1989**, *40*, 5092–5102, DOI: 10.1103/PhysRevA.40.5092.

(24) Lee, D.; Albrecht, A. C. In *Advances in Infrared and Raman Spectroscopies*; Clark, R., Hester, R., Eds.; Wiley: New York, 1985; pp 179–213.

(25) Besemann, D. M.; Condon, N. J.; Murdoch, K. M.; Zhao, W.; Meyer, K. A.; Wright, J. C. Interference, dephasing, and vibrational coupling effects between co-

herence pathways in doubly vibrationally enhanced nonlinear spectroscopies. *Chemical Physics* **2001**, *266*, 177–195, DOI: 10.1016/s0301-0104(01)00227-0.

(26) Andrews, D. L.; Thirunamachandran, T. On three-dimensional rotational averages. *The Journal of Chemical Physics* **1977**, *67*, 5026–5033, DOI: 10.1063/1.434725.

(27) Zilian, A.; Wright, J. C. Polarization effects in four-wave mixing of isotropic samples. *Molecular Physics* **1996**, *87*, 1261–1271, DOI: 10.1080/00268979600100851.

(28) Vandenbout, D.; Muller, L. J.; Berg, M. Ultrafast Raman Echoes in Liquid Acetonitrile. *Physical Review Letters* **1991**, *67*, 3700–3703, DOI: 10.1103/PhysRevLett.67.3700.

(29) Deàk, J. C.; Iwaki, L. K.; Dlott, D. D. When vibrations interact: ultrafast energy relaxation of vibrational pairs in polyatomic liquids. *Chemical Physics Letters* **1998**, *293*, 405–411, DOI: https://doi.org/10.1016/S0009-2614(98)00814-8.

(30) Nath, S.; Urbanek, D. C.; Kern, S. J.; Berg, M. A. Simultaneous time and frequency detection in femtosecond coherent Raman spectroscopy. II. Application to acetonitrile. *Journal of Chemical Physics* **2007**, *127*, 044307, DOI: 10.1063/1.2752166.

(31) Dereka, B.; Lewis, N. H. C.; Keim, J. H.; Snyder, S. A.; Tokmakoff, A. Characterization of Acetonitrile Isotopologues as Vibrational Probes of Electrolytes. *Journal of Physical Chemistry B* **2022**, *126*, 278–291, DOI: 10.1021/acs.jpcb.1c09572.

(32) Kochanov, R.; Gordon, I.; Rothman, L.; Shine, K.; Sharpe, S.; Johnson, T.; Wallington, T.; Harrison, J.; Bernath, P.; Birk, M. et al. Infrared absorption cross-sections in HITRAN2016 and beyond: Expansion for climate, environment, and atmospheric applications. *Journal of Quantitative Spectroscopy and Radiative Transfer* **2019**, *230*, 172–221, DOI: 10.1016/j.jqsrt.2019.04.001.

(33) Kohler, D. D.; Thompson, B. J.; Wright, J. C. Resonant Third-Order Susceptibility of PbSe Quantum Dots Determined by Standard Dilution and Transient Grating

Spectroscopy. *The Journal of Physical Chemistry C* **2018**, *122*, 18086–18093, DOI: 10.1021/acs.jpcc.8b04462.

(34) Kamga, F. M.; Sceats, M. G. Pulse-sequenced coherent anti-Stokes Raman scattering spectroscopy: a method for suppression of the nonresonant background. *Opt. Lett.* **1980**, *5*, 126–128, DOI: 10.1364/OL.5.000126.

(35) Carlson, R. J.; Wright, J. C. Absorption and Coherent Interference Effects in Multiply Resonant Four-Wave Mixing Spectroscopy. *Applied Spectroscopy* **1989**, *43*, 1195–1208, DOI: 10.1366/0003702894203408.

(36) Mathew, N. A.; Rickard, M. A.; Kornau, K. M.; Pakoulev, A. V.; Block, S. B.; Yurs, L. A.; Wright, J. C. Coherent Multidimensional Vibrational Spectroscopy of Representative N-Alkanes. *The Journal of Physical Chemistry A* **2009**, *113*, 9792–9803, DOI: 10.1021/jp905172p, PMID: 19725584.

(37) Kornau, K. M.; Rickard, M. A.; Mathew, N. A.; Pakoulev, A. V.; Wright, J. C. Multiresonant Coherent Multidimensional Vibrational Spectroscopy of Aromatic Systems: Pyridine, a Model System. *The Journal of Physical Chemistry A* **2011**, *115*, 4054–4062, DOI: 10.1021/jp1104856, PMID: 21434678.

(38) Glass, W. K.; Pullin, A. D. E. Overtone and Combination-Tone Spectra of Methyl Compounds Part 1. - C_{3v} Molecules, Observed Regularities. *Transactions of the Faraday Society* **1963**, *59*, 25–42, DOI: 10.1039/tf9635900025.

(39) Pace, E. L.; Noe, L. J. Infrared Spectra of Acetonitrile and Acetonitrile-d_3. *Journal of Chemical Physics* **1968**, *49*, 5317–5325, DOI: 10.1063/1.1670050.

(40) Fermi, E. Über den Ramaneffekt des Kohlendioxyds. *Zeitschrift für Physik* **1931**, *71*, 250–259, DOI: 10.1007/BF01341712.

(41) Darling, B. T.; Dennison, D. M. The Water Vapor Molecule. *Phys. Rev.* **1940**, *57*, 128–139, DOI: 10.1103/PhysRev.57.128.

(42) Nestor, J. R.; Lippincott, E. R. The effect of the internal field on Raman scattering cross sections. *Journal of Raman Spectroscopy* **1973**, *1*, 305–318, DOI: 10.1002/jrs.1250010309.

(43) Wright, J. C.; Condon, N. J.; Murdoch, K. M.; Besemann, D. M.; Meyer, K. A. Quantitative modeling of nonlinear processes in coherent two-dimensional vibrational spectroscopy. *Journal of Physical Chemistry A* **2003**, *107*, 8166–8176, DOI: 10.1021/jp034018i.

(44) Donaldson, P. M. Photon echoes and two dimensional spectra of the amide I band of proteins measured by femtosecond IR - Raman spectroscopy. *Chemical Science* **2020**, *11*, 8862–8874, DOI: 10.1039/d0sc02978e.

(45) Donaldson, P. M.; Guo, R.; Fournier, F.; Gardner, E. M.; Barter, L. M. C.; Barnett, C. J.; Gould, I. R.; Klug, D. R.; Palmer, D. J.; Willison, K. R. Direct identification and decongestion of Fermi resonances by control of pulse time ordering in two-dimensional IR spectroscopy. *Journal of Chemical Physics* **2007**, *127*, 114513, DOI: 10.1063/1.2771176.

(46) Boyle, E. S.; Neff-Mallon, N. A.; Handali, J. D.; Wright, J. C. Resonance IR: A Coherent Multidimensional Analogue of Resonance Raman. *Journal of Physical Chemistry A* **2014**, *118*, 3112–3119, DOI: 10.1021/jp5018554.

(47) Mathew, N. A.; Yurs, L. A.; Block, S. B.; Pakoulev, A. V.; Kornau, K. M.; Sibert, E. L.; Wright, J. C. Fully and Partially Coherent Pathways in Multiply Enhanced Odd-Order Wave-Mixing Spectroscopy. *Journal of Physical Chemistry A* **2010**, *114*, 817–832, DOI: 10.1021/jp9088063.

(48) Dereka, B.; Yu, Q.; Lewis, N. H. C.; Carpenter, W. B.; Bowman, J. M.; Tokmakoff, A. Crossover from hydrogen to chemical bonding. *Science* **2021**, *371*, 160–164, DOI: 10.1126/science.abe1951.

(49) Morrow, D. J.; Kohler, D. D.; Zhao, Y. Z.; Jin, S.; Wright, J. C. Triple sum frequency pump-probe spectroscopy of transition metal dichalcogenides. *Physical Review B* **2019**, *100*, 235303, DOI: 10.1103/PhysRevB.100.235303.

(50) Piontek, S. M.; Borguet, E. Vibrational Dynamics at Aqueous-Mineral Interfaces. *Journal of Physical Chemistry C* **2022**, *126*, 2307–2324, DOI: 10.1021/acs.jpcc.1c08563.

(51) Ahmed, M. K.; Henry, B. R. Intensity distribution in the overtone spectra of methyl halides: A local mode analysis of the spectra of methyl halides and methyl cyanide. *Journal of Chemical Physics* **1987**, *87*, 3724–3730, DOI: 10.1063/1.452977.

(52) Vosko, S. H.; Wilk, L.; Nusair, M. Accurate spin-dependent electron liquid correlation energies for local spin density calculations: a critical analysis. *Canadian Journal of Physics* **1980**, *58*, 1200–1211, DOI: 10.1139/p80-159.

(53) Lee, C. T.; Yang, W. T.; Parr, R. G. Development of the Colle-Salvetti correlation-energy formula into a functional of the electron density. *Physical Review B* **1988**, *37*, 785–789, DOI: 10.1103/PhysRevB.37.785.

(54) Becke, A. D. Density-functional thermochemistry. III. The role of exact exchange. *Journal of Chemical Physics* **1993**, *98*, 5648–5652, DOI: 10.1063/1.464913.

(55) Stephens, P. J.; Devlin, F. J.; Chabalowski, C. F.; Frisch, M. J. Ab Initio Calculation of Vibrational Absorption and Circular Dichroism Spectra Using Density Functional Force Fields. *Journal of Physical Chemistry* **1994**, *98*, 11623–11627, DOI: 10.1021/j100096a001.

(56) Frisch, M. J.; Trucks, G. W.; Schlegel, H. B.; Scuseria, G. E.; Robb, M. A.; Cheeseman, J. R.; Scalmani, G.; Barone, V.; Petersson, G. A.; Nakatsuji, H. et al. Gaussian 16 Rev. C.01. 2016.

(57) Boyer, M. A.; McCoy, A. B. A flexible approach to vibrational perturbation theory using sparse matrix methods. *Journal of Chemical Physics* **2022**, *156*, 054107, DOI: 10.1063/5.0080892.

(58) Boyer, M. A.; McCoy, A. B. A wave function correction-based approach to the identification of resonances for vibrational perturbation theory. *Journal of Chemical Physics* **2022**, *157*, 164113, DOI: 10.1063/5.0121915.

(59) Boyer, M. A. PyVibPTn. **2022**, DOI: 10.5281/zenodo.7083195.

(60) McDonnell, R. P.; Devulapalli, V. S. D.; Choi, T. H.; McDonnell, L.; Goodenough, I.; Das, P.; Rosi, N. L.; Johnson, J. K.; Borguet, E. Anomalous Infrared Intensity Behavior of Acetonitrile Diffused into UiO-67. *Chemistry of Materials* **2023**, *35*, 8827–8839, DOI: 10.1021/acs.chemmater.3c00639.

(61) Cho, M. Coherent two-dimensional optical spectroscopy. *Chemical Reviews* **2008**, *108*, 1331–1418, DOI: 10.1021/cr078377b.

(62) Guo, R.; Fournier, F.; Donaldson, P. M.; Gardner, E. M.; Gould, I. R.; Klug, D. R. Detection of complex formation and determination of intermolecular geometry through electrical anharmonic coupling of molecular vibrations using electron-vibration-vibration two-dimensional infrared spectroscopy. *Physical Chemistry Chemical Physics* **2009**, *11*, 8417–8421, DOI: 10.1039/b910804a.

(63) Boyle, E. S.; Neff-Mallon, N. A.; Wright, J. C. Triply Resonant Sum Frequency Spectroscopy: Combining Advantages of Resonance Raman and 2D-IR. *Journal of Physical Chemistry A* **2013**, *117*, 12401–12408, DOI: 10.1021/jp409377a.

(64) Molesky, B. P.; Giokas, P. G.; Guo, Z. K.; Moran, A. M. Multidimensional resonance raman spectroscopy by six-wave mixing in the deep UV. *Journal of Chemical Physics* **2014**, *141*, 114202, DOI: 10.1063/1.4894846.

(65) Handali, J. D.; Sunden, K. F.; Thompson, B. J.; Neff-Mallon, N. A.; Kaufman, E. M.; Brunold, T. C.; Wright, J. C. Three Dimensional Triply Resonant Sum Frequency Spectroscopy Revealing Vibronic Coupling in Cobalamins: Toward a Probe of Reaction Coordinates. *Journal of Physical Chemistry A* **2018**, *122*, 9031–9042, DOI: 10.1021/acs.jpca.8b07678.